

New aspects of the metal-insulator transition in single-domain vanadium dioxide nanobeams

Jiang Wei, Zenghui Wang, Wei Chen and David H. Cobden*

Many strongly correlated electronic materials have a domain structure that greatly influences the bulk properties and obscures the fundamental properties of the homogeneous material. Nanoscale samples, on the other hand, can be smaller than the characteristic domain size, thus making it possible to explore these fundamental properties in detail. Here, we report new aspects of the metal-insulator transition^{1–3}, studied in single-domain vanadium dioxide nanobeams^{4–6}. We have observed supercooling of the metallic phase by 50 °C, an activation energy in the insulating phase that is consistent with the optical gap, and a connection between the metal-insulator transition and the equilibrium carrier density in the insulating phase. Our devices also provide a nanomechanical method for determining the transition temperature, enable measurements on individual metal-insulator interphase walls to be made, and allow general investigations of phase transitions in quasi-one-dimensional geometries.

Bulk vanadium dioxide, VO₂, is a poor metal above a critical temperature T_c of 68 °C, and below this temperature is a semiconductor with an optical gap⁷ E_g of 0.6 eV. The transition to the metal can be induced very rapidly and has recently been studied intensively using ultrafast techniques^{8–14}. The lattice in the metallic phase has the rutile structure, with the vanadium ions arranged in periodic chains parallel to the *c*-axis. In the insulating phase these are distorted into dimerized zigzag chains, resulting in a monoclinic structure known as M1. Many factors indicate that the transition involves strong electron–electron correlations, as in a Mott transition. These include the anomalously low conductivity and other properties of the metal^{15–17}, the fact that band structure calculations fail to yield the insulator bandgap^{3,18}, the fact that an intermediate M2 structure, which can be stabilized by stress¹⁹ or doping²⁰, is insulating in spite of having undimerized vanadium chains²¹, and the dependence on excitation power in optical experiments, which indicates sensitivity to excited carrier density^{12,13,22}. However, the nature of the transition is still quite unclear even half a century after its discovery¹, and potential applications in electrical²³ and optical²⁴ switching or detection, for example, remain unrealized. The blame for this falls largely on the domain structure produced on passing through the metal–insulator transition (MIT)²⁵, which leads to irreproducibility between samples (properties such as resistivity are very sensitive to the arrangement of domains), broadening and hysteresis of the characteristics, and non-uniform stresses producing mechanical degradation¹⁵. All these problems are absent in our nanobeam devices, which are smaller than the characteristic domain size.

The nanobeams were grown directly on oxidized silicon wafers by a physical vapour transport technique based on that introduced by Park's group^{4,5}. The substrate was placed in 20 mbar argon carrier gas downstream from a granular VO₂ source in a tube furnace at 1,000 °C for 30 min. Each nanobeam is a single crystal elongated along the rutile *c*-axis. The length can be hundreds of micrometres

and the cross-section is roughly rectangular, the width W ranging down to 50 nm and thickness H down to 15 nm, as determined by atomic force microscopy. As reported by others⁵, on warming, quasiperiodic thin stripes of darker metallic phase can be seen to appear around 65 °C in an optical microscope (Fig. 1a). These stripes then widen and eventually merge, and the insulating phase disappears by ~105 °C. This behaviour results from strain caused by firm attachment to the SiO₂ substrate. A fully insulating nanobeam is under compressive axial strain, whereas a fully metallic one, having a smaller equilibrium *c*-axis lattice constant, is under tension. Alternation of metallic and insulating regions reduces the average strain at the cost of creating interphase walls. Park's group⁵ has also found that if the nanobeams are released from the substrate, completely relieving the strain, the transition becomes sudden with no stable domain pattern formation.

Here, rather than eliminating the axial strain, we take advantage of it. Using electron-beam or optical lithography we patterned a series of electron-beam evaporated metal contacts (typically 10 nm vanadium under 400 nm gold) onto each nanobeam, and then immersed it in buffered oxide etch to remove the 1- μ m-thick SiO₂ beneath it where it was not covered by metal, thereby suspending the nanobeam sections between the contacts. The behaviour of many of the resulting devices, under repeated cycling in air between room temperature T_{room} and 120 °C, is reproducible over a period of months. Unlike bulk crystals, these nanobeams do not degrade or fracture. At T_{room} , shorter sections are straight and longer ones are buckled (see Fig. 1b). This is consistent with the behaviour of clamped beams, in which Euler buckling occurs when the compressive axial stress P exceeds a critical value P_b , which is smaller for longer beams. Firm adhesion to the substrate under the contacts provides the clamping. After buckling, the compressive strain η is much smaller and the nanobeam adopts approximately its natural length L_0 . By taking L_0 to be the length along the curved profile of a buckled section measured in an atomic force microscope, and calling the contact separation L , we find that the substrate-induced strain in most nanobeams at T_{room} is $\eta_0 = (L_0 - L)/L = 0.4 \pm 0.1\%$. This is consistent with an 0.7% thermal contraction of the rutile VO₂ relative to the substrate followed by a 1.1% expansion on conversion to the M1 form during cooling from the growth temperature^{5,26,27}.

Seen in an optical microscope, between ~68 and 105 °C every segment of each nanobeam is unbuckled, and in nearly all cases each consists of one metallic and one insulating region coexisting and separated by a single interphase wall (see Fig. 1c). As T increases, the fraction x of the insulating phase, plotted in Fig. 1d, decreases steadily until at a temperature T_m in the vicinity of 105 °C the nanobeam becomes fully metallic. This behaviour can be understood by noting that given fixed L , once the nanobeam begins to convert from insulator to metal its equilibrium length L_0 decreases because of the shorter *c*-axis of the metal, and therefore so do both η and P . At any particular T the fraction x of insulator adjusts so that P is appropriate for the two phases to coexist, that

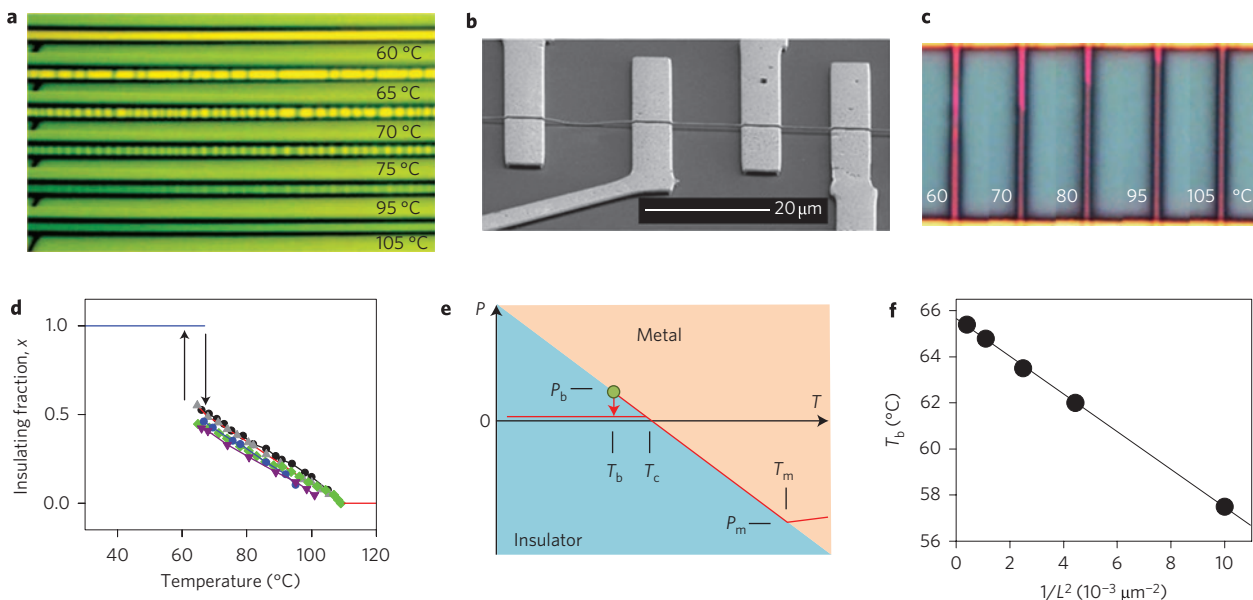


Figure 1 | Metal-insulator transition in VO₂ nanobeams studied by microscopy. **a**, Six images of a 40- μm -long part of a single nanobeam attached as grown to an SiO₂ substrate, taken at the indicated temperatures during warming, showing metallic domains (darker) appearing, widening and merging. **b**, Scanning electron microscopy image of a suspended nanobeam device showing that longer sections are buckled at room temperature. **c**, Five images of one suspended nanobeam between contacts at the top and bottom separated by 20 μm . Above 68 $^{\circ}\text{C}$ it contains a single metallic domain (grey), which grows on warming until the insulating domain (purple) disappears at $\sim 105^{\circ}\text{C}$. **d**, Plot of the insulating fraction x versus T for six suspended nanobeams of various dimensions, showing that, to within a constant offset, x always has the same linear variation in coexistence. **e**, Sketch of the phase diagram indicating part of the trajectory (red) followed on a temperature cycle starting at room temperature (left of figure). The vertical axis is uniaxial pressure P . The green circle indicates the point at which the nanobeam buckles on cooling. **f**, Plot of buckling temperature T_b versus inverse square length for a nanobeam (thickness $H = 0.18 \mu\text{m}$, width $W = 0.9 \mu\text{m}$) yielding a straight line for which the y -intercept should be T_c .

is, to lie on the phase boundary line between insulator and metal in the (P, T) -plane, as sketched in Fig. 1e. The stress P should be zero at $T = T_c$ and negative (tensile) at higher T , explaining why all nanobeams become straight above $\sim 68^{\circ}\text{C}$.

The nanobeam thus provides a one-dimensional analogue of the three-dimensional situation of water held at constant volume near 0°C . In this case, too, the low- T phase (ice) has higher volume and lower symmetry than the high- T phase (liquid water), and the fraction x of ice decreases as T increases in a corresponding way. It is also worth noting that in the coexistence regime the nanobeam has zero axial stiffness, just as the ice–water mixture has diverging isothermal compressibility.

If we assume the Young’s modulus E is the same for both phases then the strain $\eta(T)$ is uniform along the nanobeam and the equilibrium phase boundary line $P(T)$ is determined by

$$P(T)/E = \eta(T) = \alpha(x - x_c) + K(T - T_c) \quad (1)$$

The first term on the right represents interconversion between the phases, where α is the fractional increase in rutile c -axis length going from metal to insulator and x_c is the insulating fraction at $T = T_c$. The second term represents differential thermal expansion of the VO₂ relative to the silicon substrate. It is an order of magnitude smaller than the first term, K being about $+2.0 \times 10^{-5} \text{ }^{\circ}\text{C}^{-1}$ and assumed the same for both phases^{5,26,27}.

According to equation (1), for every nanobeam x should have the same variation with T to within an offset x_c that depends on the built-in strain relative to the substrate and may vary with growth conditions. The data in Fig. 1d agree well with this prediction, supporting the assumptions made above. Moreover, we observe that $x(T)$ is nearly a straight line, with $dx/dT = -(1.10 \pm 0.05) \times 10^{-2} \text{ }^{\circ}\text{C}^{-1}$. This implies that the phase boundary line is nearly

straight over the experimental temperature range so that we can simply write

$$P(T)/E = \beta(T - T_c) \quad (2)$$

where $\beta = \alpha dx/dT + K$ is the (negative) rate of change of strain with temperature. According to equation (2), P will become positive when a nanobeam in coexistence is cooled below T_c , and upon further cooling we expect the nanobeam to buckle at the temperature T_b , for which $P(T_b) = P_b$. Using the Euler expression for the buckling pressure of a doubly clamped beam, $P_b = (\pi^2 E/3)H^2/L^2$, we then have

$$\beta(T_b - T_c) = (\pi^2/3)H^2/L^2 \quad (3)$$

Equation (3) predicts that a plot of T_b versus $1/L^2$ will yield a straight line with y -intercept T_c . We construct such a plot in Fig. 1f for a series of sections of a nanobeam of thickness $H = 180 \pm 5 \text{ nm}$. The data are indeed well fitted by the straight line shown, with y -intercept $T_c = 65.7 \pm 0.2^{\circ}\text{C}$.

This represents a completely new way of measuring the transition temperature, making use of coupling of the phase transition to nanomechanical motion. Unlike other methods it is independent of hysteresis at the transition. In fact, the more general procedure of finding $\lim_{L \rightarrow \infty} (T_b)$ should yield T_c independently of the assumptions made above, provided only that the phase boundary is well behaved. This could be used, for example, to methodically study variations in the phase boundary between samples or in response to modified external conditions.

We can also use equation (3) to obtain β from the slope $dT_b/d(1/L^2) = -820 \pm 20 \text{ }^{\circ}\text{C } \mu\text{m}^2$ of the line, giving $\beta = (\pi^2 H^2/3)/[\partial T_b/\partial(1/L^2)] = (-13 \pm 1) \times 10^{-5} \text{ }^{\circ}\text{C}^{-1}$. Using

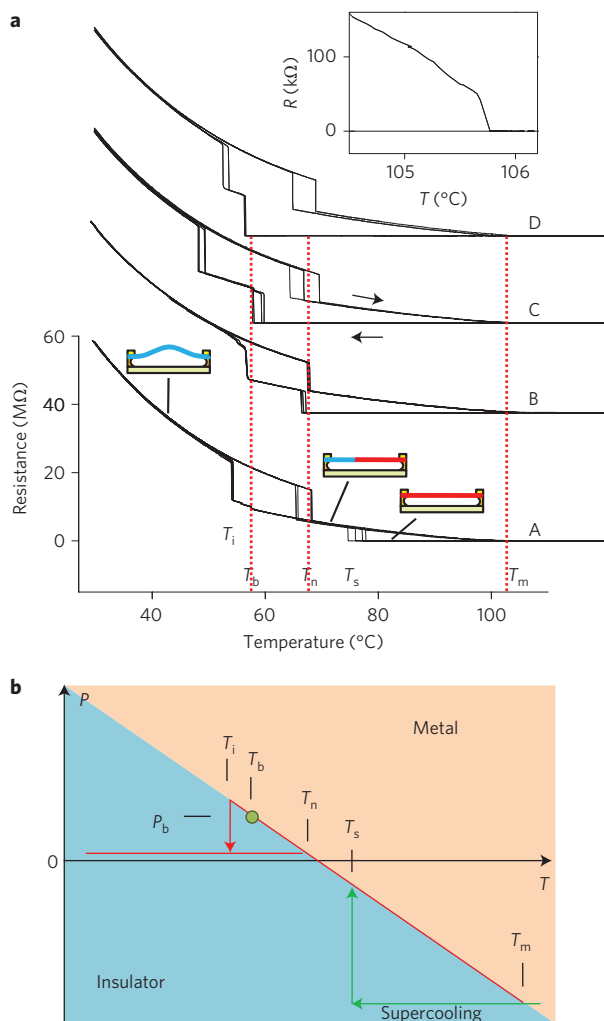


Figure 2 | Electrical resistance versus temperature. **a**, Characteristics of four sections, designated A–D, of the same nanobeam, each having dimensions $L = 26 \mu\text{m}$, $H = 0.25 \mu\text{m}$ and $W = 0.7 \mu\text{m}$. The three stable states of each section are indicated by the sketches: buckled and fully insulating (blue), straight and fully metallic (red), or coexisting (part blue, part red). Inset: a repeatable small jump of ~ 50 kΩ is seen as the insulator disappears near T_m . **b**, Corresponding phase diagram, as in Fig. 1e. The red line indicates the trajectory followed by section A. On warming from room temperature (left of figure) the nanobeam unbuckles and jumps from fully insulating to coexistence at T_n , and becomes fully metallic at T_m . On cooling it supercools to T_s (green line) at which the insulator nucleates, it buckles downwards at T_b (green circle), and it then buckles upwards and becomes fully insulating at T_i .

the estimate²⁸ $E \approx 140$ GPa, we can then quantify the stress in the nanobeam: the phase boundary slope is $\beta E \approx -18$ MPa °C⁻¹, and the largest tension, reached at $T = T_m \approx 110$ °C, is $P_m = \beta E(T_m - T_c) \approx -0.7$ GPa. For $T > T_m$ the nanobeam is fully metallic and thermal expansion causes the tension to decrease again, at a rate $dP/dT = KE \approx +2.5$ MPa °C⁻¹, as indicated in Fig. 1e. Also, using this value for β we find $\alpha = (\beta - K)/(dx/dT) = 1.36 \pm 0.15\%$. The discrepancy with the accepted value³ of $\alpha = 1.0\%$ could be partly due to the phases having different elastic moduli or to the intermediate M2 insulating phase (see below).

Measurements of the two-terminal electrical resistance R in the coexistence regime yield a number of interesting results. Figure 2a shows the characteristics on repeated thermal cycling of four nominally equal sections (A–D) of a single nanobeam. Each comprises smooth R versus T curves punctuated by sudden jumps. On warming from

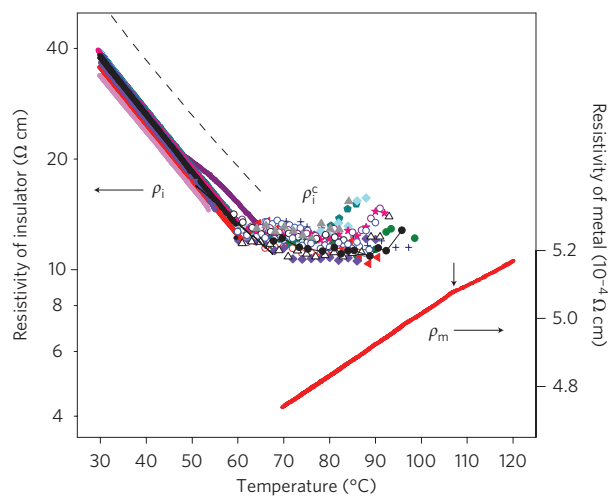


Figure 3 | Collected resistivity measurements for ten nanobeams of various dimensions. The insulator resistivity ρ_i shows an activation energy E_a of 0.30 eV (dashed line is $e^{-E_a/kT}$). Plotted using symbols are measurements of the resistivity ρ_i^c of the insulator in coexistence. To within error they all show a temperature-independent value of 12 ± 2 Ω cm. The metal resistivity ρ_m was obtained from one section of a nanobeam ($H = 0.18 \mu\text{m}$, $W = 0.9 \mu\text{m}$, $L = 30 \mu\text{m}$). Two other sections of the same nanobeam (with $L = 20$ and $50 \mu\text{m}$) gave almost identical results. The error in ρ_m due to uncertainty in the cross-section is estimated to be 25%. The values of ρ_m for temperatures below the kink (small arrow) are in the supercooled regime.

T_{room} , R initially decreases in a semiconducting manner. It drops sharply at a temperature $T_n \approx 65$ – 68 °C when a metallic region appears and the nanobeam becomes straight. Subsequently, in the coexistence regime, as the insulating region shrinks R decreases steadily to a much smaller value at $T_m \approx 105$ °C at which the insulator disappears. The coexistence curve is reproducible on sweeping up and down at 6 °C min⁻¹ as long as T is kept below T_m . On the other hand, on cooling from above T_m , each section remains fully metallic down to a lower temperature T_s at which an insulating region suddenly appears and R jumps up to the coexistence curve. T_s varies greatly between sections, from 78 °C (section A) to 55 °C (section D). During further cooling, R increases smoothly until the nanobeam buckles at $T_b = 57.5$ °C. Below that, the temperature T_i at which R returns to the insulating curve also varies, as several conformations are possible after the nanobeam initially buckles downwards and collides with the substrate. When sweeping at 6 °C min⁻¹, T_s and T_n vary within a range of 2 – 5 °C between sweeps, whereas T_b and T_m are reproducible to within the measurement accuracy of ~ 0.1 °C.

The supercooling of the homogeneous, uniformly stressed metallic phase to T_s , which can be more than 50 °C below the phase boundary, is represented by the green lines on the phase diagram in Fig. 2b. This intrinsic supercooling (as opposed to the persistence of metallic domains due to inhomogeneous strain fields in larger samples) is much larger than has been reported previously⁵ and indicates high crystal uniformity. The large variations in T_s between nanobeams could reflect the availability of imperfections at which the insulating phase can nucleate. This system offers new opportunities for investigating the kinetics of a first-order phase transition in a quasi-one-dimensional geometry, for example by studying the process of insulator nucleation at T_s or the disappearance of the insulating domain at T_m (see inset to Fig. 2a).

In Fig. 3 we plot the resistivity ρ_i (along the rutile c -axis) of a number of nanobeams in their fully insulating state obtained simply using $\rho = RA/L$, where $A = WH$. Studies of the dependence on L have shown that contact resistance is negligible. ρ_i is

consistent between samples and its T dependence gives an activation energy $E_a = 0.30 \pm 0.01$ eV, indicated by the dashed line. Interestingly, this activation energy corresponds to that expected for an intrinsic semiconductor with precisely the established optical gap⁷ $E_g = 0.60$ eV of VO_2 . This is in contrast with the anomalously large and sample-dependent activation energies of up to 0.45 eV reported in the literature¹⁵ on bulk insulating VO_2 , which are most likely influenced by domain structure or imperfections that are absent in the nanobeams.

We also plot the resistivity ρ_m of the metallic phase obtained in the same way for one nanobeam in its fully metallic state. Consistent with the literature¹⁶ we find that ρ_m increases slowly with T and that at the transition $\rho_i \approx 2 \times 10^4 \rho_m$. The kink in ρ_m at 107 °C, indicated by an arrow, occurs at the boundary between the supercooled and stable metallic phase. We do not know its origin, although we note that recent experiments have indicated that structural transitions may occur within the metallic phase under hydrostatic pressure²⁹ or transiently after ultrafast excitation¹⁰.

In the coexistence regime we expect R to have four contributions:

$$R = x\rho_i^c L/A + (1-x)\rho_m^c L/A + R_c + R_{dw} \quad (4)$$

where ρ_i^c and ρ_m^c are the insulator and metal resistivities in coexistence, and R_c and R_{dw} are the resistances of the contact to the insulator and of the domain wall, respectively. Because $\rho_i \gg \rho_m$, the second term is negligible. At T_m when the insulating domain disappears, there is usually a small sharp drop in R of around 50 k Ω (see inset to Fig. 2a). We have yet to determine whether this reflects the resistance of the domain wall, the minimum insulating domain size, or the contact to the insulator, but in any case it implies that $R_c + R_{dw} \lesssim 50$ k Ω . Because R is usually greater than 1 M Ω for measurable x , to good accuracy we can thus write

$$R = \rho_i^c xL/A \quad (5)$$

As a result, the resistance can act as a probe of the position xL of the interphase wall. We find that R can be stable to within 0.1%, limited by the thermal stage stability; hence it can be used to detect motion of the wall with an accuracy of less than 10 nm in a device with $L = 10$ μm , offering the possibility of detecting small effects of perturbations such as electric field on the transition. Applying this idea, we found no change in R on applying up to 50 V to the silicon substrate, indicating that the screening length within the semiconductor is less than the minimum nanobeam thickness, ~ 30 nm, and implying that Mott transistor action²³ will be difficult to achieve.

Most interestingly of all, by using equation (5) we can determine ρ_i^c from R using values of x obtained by optical inspection. The results are included in Fig. 3. We find that $\rho_i^c = 12 \pm 2$ Ω cm for all the nanobeams, independent of T to within measurement error. This is in sharp contrast with the activated behaviour of ρ_i , which strongly suggests carrier activation across an unchanging gap. It implies that the carrier density in the insulator becomes independent of T once the nanobeam enters coexistence; that is, in coexistence the changing strain causes the gap to increase in just such a way as to counteract the effect of thermal activation on the carrier density. In other words, the phase boundary corresponds to a contour of constant insulator carrier density in the P - T plane.

This remarkable result is unlikely to be a coincidence, especially considering recent evidence that the excited carrier density in the insulator is important when the transition is induced optically^{12,13,22}. Rather, it implies that the transition temperature is closely linked to the equilibrium carrier density in the insulating phase. This is consistent with a driving role for electron-electron interactions in the MIT, as in a Mott transition that occurs when the density-dependent screening reaches a critical strength. In contrast, a phonon-driven mechanism would not be expected to be sensitive to the non-degenerate carrier density in the insulator.

Metal-insulator transitions have been studied in bulk systems for decades and are still not fully understood. As reported here, the greatly improved reproducibility, uniformity and level of control that is possible in single-domain samples can shed new light on such transitions and other aspects of strongly correlated electron physics. Further work is ongoing to understand the various new phenomena that have been observed in VO_2 nanobeams, including the appearance of the intermediate M2 insulating state during the transition between the M1 and metallic phases, which among other things explains the larger-than-expected change α in the unit cell length reported above.

Received 11 February 2009; accepted 5 May 2009;
published online 24 May 2009

References

- Morin, F. J. Oxides which show a metal-to-insulator transition at the Neel temperature. *Phys. Rev. Lett.* **3**, 34–36 (1959).
- Mott, N. F. *Metal-Insulator Transitions*, 2nd edn (CRC, 1990).
- Eyert, V. The metal-insulator transitions of VO_2 : a band theoretical approach. *Annalen Der Physik* **11**, 650–702 (2002).
- Guiton, B. S., Gu, Q., Prieto, A. L., Gudiksen, M. S. & Park, H. Single-crystalline vanadium dioxide nanowires with rectangular cross-sections. *J. Am. Chem. Soc.* **127**, 498–499 (2005).
- Wu, J. Q. *et al.* Strain-induced self organization of metal-insulator domains in single-crystalline VO_2 nanobeams. *Nano Lett.* **6**, 2313–2317 (2006).
- Gu, Q., Falk, A., Wu, J. Q., Lian, O. Y. & Park, H. Current-driven phase oscillation and domain-wall propagation in $\text{W}_x\text{V}_{1-x}\text{O}_2$ nanobeams. *Nano Lett.* **7**, 363–366 (2007).
- Verleur, H. W., Barker, A. S. & Berglund, C. N. Optical properties of VO_2 between 0.25 and 5 eV. *Phys. Rev.* **172**, 788–798 (1968).
- Becker, M. F., Buckman, A. B. & Walsler, R. M. Femtosecond laser excitation of the semiconductor-metal phase transition in VO_2 . *Appl. Phys. Lett.* **65**, 1507–1509 (1994).
- Petrov, G. I., Yakovlev, V. V. & Squier, J. A. Nonlinear optical microscopy analysis of ultrafast phase transformation in vanadium dioxide. *Opt. Lett.* **27**, 655–657 (2002).
- Kim, H. T. *et al.* Monoclinic and correlated metal phase in VO_2 as evidence of the Mott transition: Coherent phonon analysis. *Phys. Rev. Lett.* **97**, 266401 (2006).
- Cavalleri, A., Rini, M. & Schoenlein, R. W. Ultra-broadband femtosecond measurements of the photo-induced phase transition in VO_2 : From the mid-IR to the hard X-rays. *J. Phys. Soc. Jpn* **75**, 011004 (2006).
- Hilton, D. J. *et al.* Enhanced photosusceptibility near T_c for the light-induced insulator-to-metal phase transition in vanadium dioxide. *Phys. Rev. Lett.* **99**, 226401 (2007).
- Baum, P., Yang, D. S. & Zewail, A. H. 4D visualization of transitional structures in phase transformations by electron diffraction. *Science* **318**, 788–792 (2007).
- Kubler, C. *et al.* Coherent structural dynamics and electronic correlations during an ultrafast insulator-to-metal phase transition in VO_2 . *Phys. Rev. Lett.* **99**, 116401 (2007).
- Berglund, C. N. & Guggenheim, H. J. Electronic properties of VO_2 near the semiconductor-metal transition. *Phys. Rev.* **185**, 1022–1033 (1969).
- Allen, P. B., Wentzcovitch, R. M., Schulz, W. W. & Canfield, P. C. Resistivity of the high-temperature metallic phase of VO_2 . *Phys. Rev. B* **48**, 4359–4363 (1993).
- Qazilbash, M. M. *et al.* Correlated metallic state of vanadium dioxide. *Phys. Rev. B* **74**, 205118 (2006).
- Wentzcovitch, R. M., Schulz, W. W. & Allen, P. B. VO_2 : Peierls or Mott-Hubbard? A view from band theory. *Phys. Rev. Lett.* **72**, 3389–3392 (1994).
- Pouget, J. P., Launois, H., Dhaenens, J. P., Merenda, P. & Rice, T. M. Electron localization induced by uniaxial stress in pure VO_2 . *Phys. Rev. Lett.* **35**, 873–875 (1975).
- Marezio, M., McWhan, B., Dernier, P. D. & Remeika, J. P. Structural aspects of metal-insulator transitions in Cr-doped VO_2 . *Phys. Rev. B* **5**, 2541–2551 (1972).
- Rice, T. M., Launois, H. & Pouget, J. P. Comment on 'VO₂: Peierls or Mott-Hubbard? A view from band theory'. *Phys. Rev. Lett.* **73**, 3042 (1994).
- Qazilbash, M. M. *et al.* Mott transition in VO_2 revealed by infrared spectroscopy and nano-imaging. *Science* **318**, 1750–1753 (2007).
- Chudnovskiy, F., Luryi, S. & Spivak, B. in *Future Trends in Microelectronics: The Nano Millennium* (Wiley-IEEE, 2002).
- Jerominek, H., Picard, F. & Vincent, D. Vanadium-oxide films for optical switching and detection. *Opt. Eng.* **32**, 2092–2099 (1993).
- Fisher, B. Metal-semiconductor domain configurations during switching of VO_2 single crystals. *J. Phys. C: Solid State Phys.* **9**, 1201–1209 (1976).
- Minomura, S. & Nagasaki, H. The effect of pressure on the metal-to-insulator transition in V_2O_4 and V_2O_3 . *J. Phys. Soc. Jpn* **19**, 131–132 (1964).

27. Kucharczyk, D. & Niklewski, T. Accurate X-ray determination of the lattice parameters and the thermal expansion coefficients of VO₂ near the transition temperature. *J. Appl. Cryst.* **12**, 370–373 (1979).
28. Tsai, K. Y., Chin, T. S. & Shieh, H. P. D. Effect of grain curvature on nano-indentation measurements of thin films. *Jpn J. Appl. Phys.* **43**, 6268–6273 (2004).
29. Arcangeletti, E. *et al.* Evidence of a pressure-induced metallization process in monoclinic VO₂. *Phys. Rev. Lett.* **98**, 196406 (2007).

Acknowledgements

We thank Anton Andreev, Marcel den Nijs, Patti Metcalf, Jungho Son, Boris Spivak, David Thouless, Oscar Vilches and Younan Xia for discussions, Volker Eyert and Hyun-tak Kim for comments on the manuscript, and Jacob Beedle, Megan Campbell and Conor Sayres for

experimental assistance. This work was supported by the Army Research Office under contract no. 48385-PH, and used facilities in the UW Nanotech Center. W.C. and Z.W. were partially supported by UW UIF Nanotech fellowships.

Author contributions

J.W. performed the experiments with assistance from Z.W., W.C. and D.H.C. D.H.C. guided the work and did the majority of the analysis and writing.

Additional information

Reprints and permission information is available online at <http://npg.nature.com/reprintsandpermissions/>. Correspondence and requests for materials should be addressed to D.H.C.